Bulletin of Volcanology (2018) 80: 27
https://doi.org/10.1007/s00445-018-1208-2

RESEARCH ARTICLE

The violent Strombolian eruption of 10 ka Pelado shield volcano, Sierra Chichinautzin, Central Mexico

A. Lorenzo-Merino[1] · M.-N. Guilbaud[1] · J. Roberge[2]

Received: 27 November 2017 / Accepted: 9 February 2018 / Published online: 23 February 2018

Abstract

Pelado volcano is a typical example of an andesitic Mexican shield with a summital scoria cone. It erupted ca. 10 ka in the central part of an elevated plateau in what is today the southern part of Mexico City. The volcano forms a roughly circular, 10-km wide lava shield with two summital cones, surrounded by up to 2.7-m thick tephra deposits preserved up to a distance of 3 km beyond the shield. New cartographic, stratigraphic, granulometric, and componentry data indicate that Pelado volcano was the product of a single, continuous eruption marked by three stages. In the early stage, a > 1.5-km long fissure opened and was active with mild explosive activity. Intermediate and late stages were mostly effusive and associated with the formation of a 250-m high lava shield. Nevertheless, during these stages, the emission of lava alternated and/or coexisted with highly explosive events that deposited a widespread tephra blanket. In the intermediate stage, multiple vents were active along the fissure, but activity was centered at the main cone during the late stage. The final activity was purely effusive. The volcano emitted > 0.9 km^3 dense-rock equivalent (DRE) of tephra and up to 5.6 km^3 DRE of lavas. Pelado shares various features with documented "violent Strombolian" eruptions, including a high fragmentation index, large dispersal area, occurrence of plate tephra, high eruptive column, and simultaneous explosive and effusive activity. Our results suggest that the associated hazards (mostly tephra fallout and emplacement of lava) would seriously affect areas located up to 25 km from the vent for fallout and 5 km from the vent for lava, an important issue for large cities built near or on potentially active zones, such as Mexico City.

Keywords Monogenetic volcanism · Shield volcano · Eruptive volume · Eruption duration · Volcanic hazards · Sierra Chichinautzin (Mexico)

Introduction

Monogenetic volcanoes are formed during a single eruption (Connor and Conway 2000; Francis and Oppenheimer 2004; de Silva and Lindsay 2015). Review papers commonly reduce this volcanism to mildly explosive, low-volume (< 1 km^3) and brief (< 1 year) eruptions that form small basaltic scoria cones associated with short lava flows in an extensional setting (Connor and Conway 2000; Vesperman and Schmincke 2000; Valentine and Gregg 2008; Valentine and Connor 2015; McGee and Smith 2016). Nevertheless, monogenetic volcanoes can display a wide array of eruptive styles, from entirely effusive, through Surtseyan, and up to violent Strombolian (e.g., MacDonald 1972; Walker 1973; Pioli et al. 2008; Guilbaud et al. 2009; Kshirsagar et al. 2015; Chevrel et al. 2016a). They can build large edifices (> 5–10 km^3) through complex and/or long-lasting eruptions (> 30 years) (Righter and Carmichael 1992; Hasenaka 1994; Zimmer et al. 2010; Chevrel et al. 2016a). They are also not typically basaltic. For example, the Michoacán-Guanajuato volcanic field, the largest monogenetic field on Earth, is dominantly andesitic (Hasenaka and Carmichael 1987; Connor and Conway 2000). Wide chemical variations may exist in the products from a single volcano, indicating complex

Editorial responsibility: C. Bonadonna

Electronic supplementary material The online version of this article (https://doi.org/10.1007/s00445-018-1208-2) contains supplementary material, which is available to authorized users.

✉ A. Lorenzo-Merino
ainhoa@geofisica.unam.mx

[1] Departamento de Vulcanología, Instituto de Geofísica, Universidad Nacional Autónoma de México, Del. Coyoacán, 04510 Ciudad de México, México

[2] Posgrado ESIA-Ticomán, Instituto Politécnico Nacional, Del. Gustavo A. Madero, 07340 Ciudad de México, México

magmatic processes occurring at the mantle and crustal levels (Németh et al. 2003; Strong and Wolff 2003; Smith et al. 2008; Roberge et al. 2015; Chevrel et al. 2016b; McGee and Smith 2016; Rasoazanamparany et al. 2016). Finally, monogenetic volcanoes occur in all tectonic settings (Le Corvec et al. 2013) and, despite the short "lifespan" of single edifices, they are of significance for studying long-term geological processes as the fields can be active for millions of years (e.g., Cas and Wright 1988; Siebe et al. 2004a; Németh 2010).

Medium-sized monogenetic shield volcanoes are important constituents of volcanic fields in different parts of the world (e.g., Snake River Plain, Idaho, USA, Greeley 1982; Michoacán-Guanajuato, Serdán-Oriental and Xalapa Volcanic Fields, Mexico, Hasenaka 1994; Rodríguez et al. 2010; Iceland, Rossi 1996; Auckland Volcanic Field, New Zealand, Shane and Smith 2000). Their convex, low-angle slopes are similar to the traditional, Hawaiian-style shields but they have smaller basal diameters (< 20 km) and heights (< 1000 m) (Williams and McBirney 1979; Whitford-Stark 1975). These types of volcanoes are ubiquitous along the active subduction-related Trans-Mexican Volcanic Belt (Righter and Carmichael 1992; Delgado Granados 1992; Hasenaka 1994; Aguirre-Díaz et al. 2006; Rodríguez et al. 2010). Their highest concentration occurs in the Michoacán-Guanajuato Volcanic Field, followed by the Sierra Chichinautzin Volcanic Field (SCVF) (Siebe et al. 2004a, 2005; Agustín-Flores et al. 2011; Chevrel et al. 2016b). The shield volcanoes in the Michoacán-Guanajuato Volcanic Field were denominated as *Mexican shields* by Hasenaka (1994) because their slopes are significantly higher (5–15°) than all of the categories defined by Whitford-Stark (1975) due to their dominantly andesitic composition. Hasenaka (1994) defined two types of Mexican shields: type A, with slope angles of around 5°, and type B, with slope angles of 10–15°.

The eruptive style, morphology, and duration of Mexican shields are poorly defined. Whereas some, such as El Metate in the Michoacán-Guanajuato Volcanic Field (Chevrel et al. 2016a, b), appear to be purely effusive, most have summital scoria cones, which indicates at least a mildly explosive component (Hasenaka and Carmichael 1985; Siebe et al. 2004a, 2005; Agustín-Flores et al. 2011; Guilbaud et al. 2015). Their large erupted volumes (0.5–10 km^3, Hasenaka 1994) suggest either longer eruption durations (> 1 year) or larger eruption rates in comparison to other, more common, smaller monogenetic volcanoes (Wood 1980; Righter and Carmichael 1992; Chevrel et al. 2016a). This is particularly relevant in areas with a high population density, where the related hazards can easily become major risks. In this respect, the possibility of formation of a new volcano of this type within the SCVF, over which the southern part of Mexico City is rapidly expanding (Fig. 1), is of particular concern.

The SCVF is a seismically active Pleistocene monogenetic field that concentrates 221 edifices in ~ 2500 km^2, including more than ten Holocene volcanoes (Figs. 1 and 2; Bloomfield 1975; Martin del Pozzo 1982; Lugo-Hubp 1984; Márquez et al. 1999; Siebe et al. 2005; Arce et al. 2013). It is located atop an elevated fault-bounded plateau (Siebe et al. 2004b), and about 15 of its edifices (e.g., Pelado, Chichinautzin, Tláloc, Chinconquiat, Teuhtli, Dos Cerros, Ocusacayo, Cuautzin, and Holotepec) are medium-sized shields (Fig. 1). Lavas from them have been analyzed compositionally and some have been dated (Bloomfield 1975; Siebe et al. 2004a, b, 2005; Schaaf et al. 2005; Straub et al. 2008, 2013; Agustín-Flores et al. 2011). However, a detailed study on the eruptive style, volume, and duration of these volcanoes is lacking. Here, we contribute to filling this gap by reconstructing the 10 ka eruption of the Pelado andesitic shield volcano (Siebe et al. 2004a, b), analyzing in detail its widespread tephra deposits. We use the results to assess the hazards related to the possible occurrence of an eruption of this type at a distance of a few kilometers from one of the most densely populated areas in the world, i.e., Mexico City, with a population of nearly 22 million and a population density of ~ 6000 inhabitants per square kilometer (Instituto Nacional de Estadística, Geografía e Informática [INEGI] 2010).

Methods

Cartography, stratigraphy, and sampling

The outlines of Pelado's edifice and surrounding volcanoes were first mapped in ArcGIS 10.1 ® with the aid of a recently developed digital elevation model from the Instituto Nacional de Estadística, Geografía e Informática (Fig. 2). This digital elevation model has 5-m horizontal resolution and is based on Light Detection and Ranging (LIDAR) data. The outlines of lavas from young volcanoes were established on the basis of surface textures and topographic changes at their margins. For older volcanoes whose lavas are buried under thick soils, topographical gradients were used to infer the extent and flow direction of their lavas. The limits of Pelado's lavas were studied in more detail by extensive fieldwork following an examination of surface textures on Google Earth's series of satellite images (1984–2016). At strategic sites located on Fig. 2, where the origin of the flow was uncertain, lava samples were collected and their crystal and vesicular texture was compared with that of well-established Pelado lava samples.

Extensive fieldwork was conducted around Pelado volcano, roughly within the area mapped on Fig. 2, in order to identify, study, and map the tephra sequence associated to the eruption, as well as to establish its stratigraphic relation with the lava shield. Detailed stratigraphic columns were elaborated at the 24 distinct sites where well-stratified, non-reworked tephra deposits from Pelado could be identified (Online Resource 1; Fig. 2). For each column, the

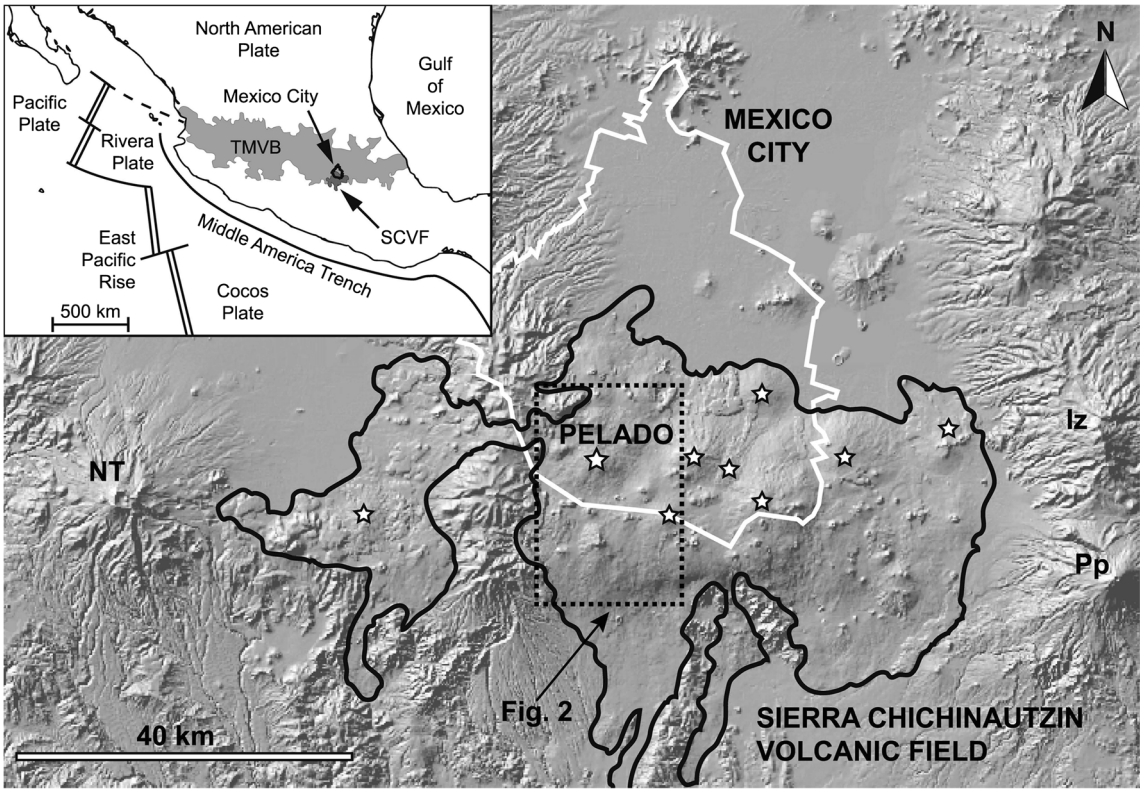

Fig. 1 Digital elevation image of the Sierra Chichinautzin volcanic field (black solid outline) and the southern limits of Mexico City (white solid outline). Stars mark the location of the edifices that are here classified as medium-sized shields, according to their height and basal diameter and following the criteria of Whitford-Stark (1975). Major stratovolcanoes such as Nevado de Toluca (NT), Iztaccihuatl (Iz), and Popocatepetl (Pp) are also shown. The black dotted rectangle shows the location of the map presented in Fig. 2. The relation of the SCVF to the tectonic context of Mexico is presented in the inset

characteristics of the distinct tephra stratigraphic layers or strata (grading, thickness, clast vesicularity, and shape) were recorded in field logs. The tephra stratigraphic columns were further subdivided into units, primarily based on systematic changes in the grain sizes and componentry of the defined strata. Representative tephra samples were taken of the strata where the tephra was fresh and not altered. At sites where lava units were intercalated with the tephra (see locations on Fig. 2), the crystal, and vesicular texture of the lava was described from the outcrop and hand samples. The columns were correlated using the established sequence of strata and units as well as distinctive marker layers. From this information, a composite tephra stratigraphic column was produced.

From the total of 48 tephra samples collected from the different sites, 14 were selected for detailed analysis in the laboratory. These mainly come from two sites where the stratigraphic columns were particularly well-preserved (sites 21 and 71, Fig. 2; Online Resource 1) These samples were dry hand-sieved in intervals of 1φ and were manually separated into distinct clast types using a × 5 magnifier lamp for sizes between – 3φ and – 1φ. For sizes finer than – 1φ, representative sub-samples were taken and separated using a binocular microscope. Thin sections of the dominant size fraction (mode) were prepared commercially by Mann Petrographics (NM, USA) and studied under petrographic and electron microscopes at the Instituto de Geofisica (UNAM, México City). The average vesicularity of each section was estimated by thin section point-counting under a petrographic microscope. Granulometry, componentry, and vesicularity data are reported in Online Resource 2.

Volume estimates

Isopach maps were produced for each major unit of the tephra stratigraphic column, interpolating between discrete thickness measurements made in the field at the sites located on Fig. 2. Sections that showed abnormal thicknesses (sites 01 and 55, Fig. 2; Online Resource 1) were not considered. The area covered by each isopach was determined using ArcGIS. The volume of the tephra deposits was calculated on the basis of an exponential fit of the "thickness" versus "isopach area" data, following Pyle (1989) (Online Resource 3). More sophisticated estimates cannot be used here because Pelado's tephra is only exposed at a distance of 5–8 km from the vent (more proximal exposures are buried under the lava shield, and more distal exposures cannot be reliably identified due to the abundance of possible sources for the tephra and the disappearance of marker layers). The exponential method is however known

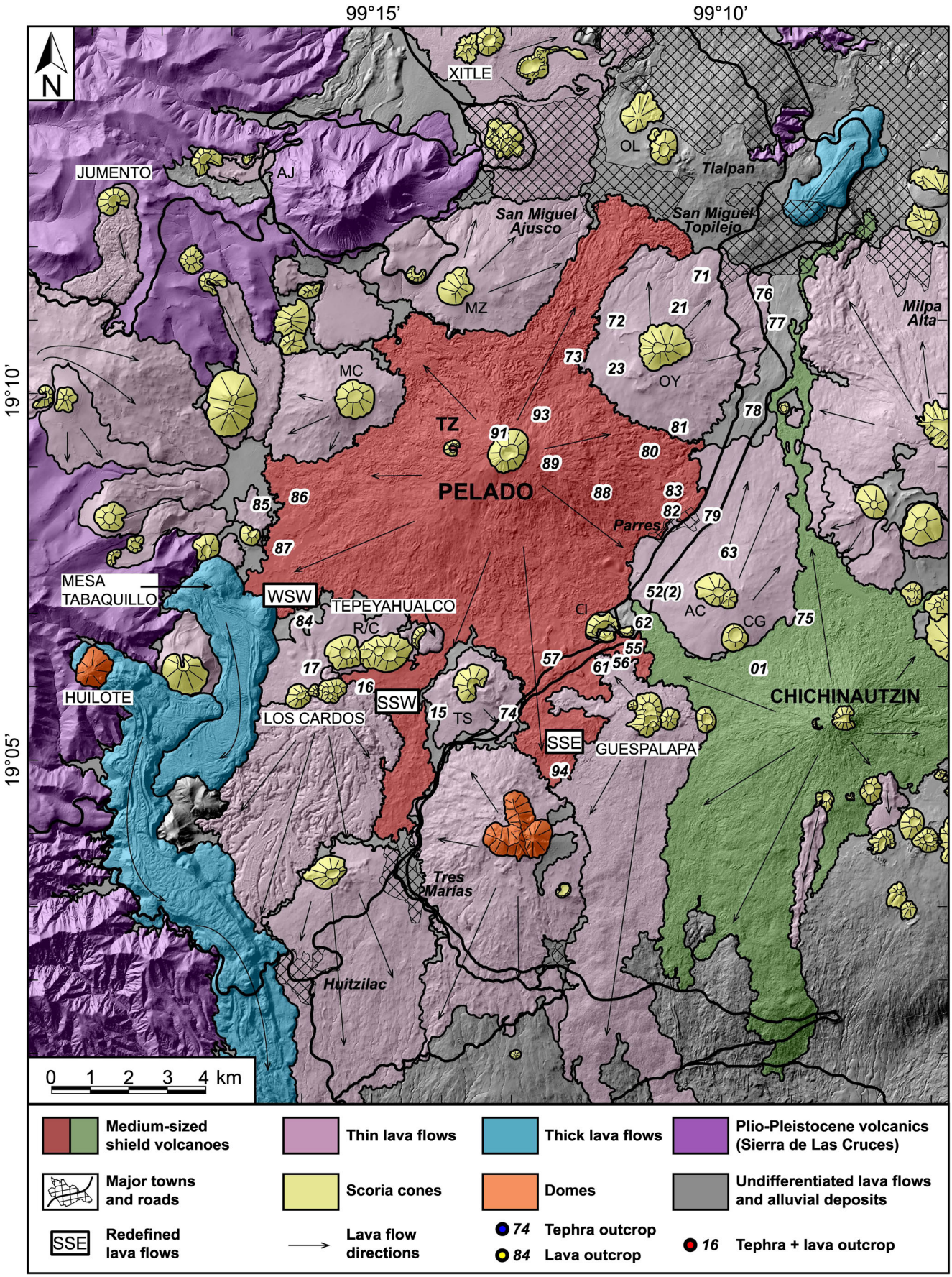
99°15'
99°10'
19°10'
19°05'
N
XITLE
OL
Tlalpan
JUMENTO
AJ
San Miguel Ajusco
San Miguel Topilejo
MZ
Milpa Alta
MC
TZ
PELADO
OY
Parres
MESA TABAQUILLO
WSW
TEPEYAHUALCO
R/C
CI
AC
CG
HUILOTE
LOS CARDOS
SSW
TS
SSE
GUESPALAPA
CHICHINAUTZIN
Tres Marías
Huitzilac
0 1 2 3 4 km
Medium-sized shield volcanoes
Thin lava flows
Thick lava flows
Plio-Pleistocene volcanics (Sierra de Las Cruces)
Major towns and roads
Scoria cones
Domes
Undifferentiated lava flows and alluvial deposits
Redefined lava flows
Lava flow directions
74 Tephra outcrop
84 Lava outcrop
16 Tephra + lava outcrop

◀ **Fig. 2** Geological map of the central-west portion of the Sierra Chichinautzin where Pelado volcano is located. The location of tephra and lava outcrops that were studied in details are shown. Holocene volcanoes (other than Pelado and Chichinautzin) are marked with white labels. AC Acopiaxco, AJ Ajusco, CI La Cima, CG Caldera El Guarda, MC Malacatepec, MZ Mezontepec, OL Ololizqui, OY Oyameyo, R/C Las Raíces/El Cajete Complex, TS Tesoyo, TZ Tzotzocol

to underestimate the volume of tephra (e.g., Pyle 1989; Bonadonna and Houghton 2005; Bonadonna and Costa, 2012) consequently; our tephra volume estimates are minimum.

The volume of the whole shield (lavas + summital cones) was calculated as the volumetric difference between the surface of the shield just after eruption (post-eruptive surface) and the topography prior to the eruption (pre-eruptive surface). First, the post-eruptive surface was reconstructed by "removing" overlapping lavas from younger volcanoes (dashed lines on Fig. 3a), interpolating 20 m contour lines across these areas and then estimating the extent of Pelado's covered lavas (Fig. 3b). Then, the pre-eruptive surface was reconstructed by interpolating 20 m contour lines across the area covered by the whole shield, taking into account the general topographic gradient towards the south (Fig. 3c). Finally, the shield volume was calculated from both reconstructed surface models (Fig. 3b, c) using the Surface Difference tool of the ArcGIS 3D Analyst ® extension package. The volume estimated by this method is probably overestimated, given the absence of proximal exposures within the shield that could confirm the pre-eruptive surface.

The volume of the exposed part of the summital cones was obtained using the Surface Volume tool of the same ArcGIS package, considering the outlines of the cones on the geological map (Fig. 2) and a flat base that was established by averaging 16 measurements of cone height. The total volume of the cones (i.e., including the parts that were buried by the lava flows) was estimated using an elliptical truncated cone formula corrected for the crater hole (Lorenzo-Merino 2016) and the pre-eruptive surface defined above (Fig. 4).

Results

Pelado volcano consists of two scoria cones, Pelado proper (180-m high, 1030-m wide, 3625 m a.s.l.) and Tzotzocol (80-m high, 390-m wide, 3406 m.a.s.l.), both of which are located at the summit of the lava shield and are henceforth referred to as "summital cones." The basal radius of the lava shield measures ~ 5 km (Fig. 2) and its slopes vary from 4° in the west to 6.5° in the east, falling between categories A and B of Mexican shields defined by Hasenaka (1994). Its surface morphology is that of a compound lava flow field composed of several flow units emplaced during the same event (Walker 1971). Distal lava flows branch from the base of the shield and fill small depressions between older cones and associated lavas, reaching up to 10 km from the vent in the south-southwest direction (Fig. 2). The full extent of these flows was not previously recognized by Siebe et al. (2004a) because they are located in depressions where thick reworked material has been deposited since their emplacement, concealing their surface features. Nevertheless, they are exposed locally and their distinct planar, sheet-like surface can be mapped on the LIDAR images. We also found that distally, these flows are overlapped by lavas from Los Cardos, Tepeyahualco, and Mesa Tabaquillo volcanoes, which are hence younger than Pelado (Fig. 2). The revised lava boundaries raise the area of the actual lava shield to 80.4 km^2, whereas Siebe et al. (2004a) had previously mapped an area of 79 km^2. The total area

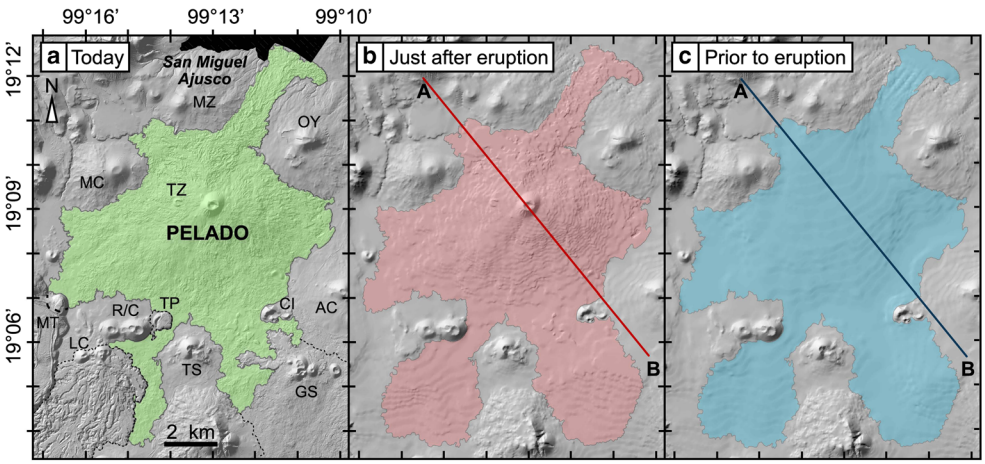

Fig. 3 Digital elevation model of the Pelado area with the successive stages in the reconstruction of the paleotopography. **a** Present topography with the exposed lavas of Pelado in green and overlapping lavas from younger volcanoes marked by dashed lines. **b** Reconstruction of the shield surface just after the eruption (post-eruptive surface, in pink). **c** Hypothetical reconstruction of the topography prior to the eruption (pre-eruptive surface) with the total area covered by the erupted lavas in blue. The solid lines in **b** and **c** show the profiles plotted in Fig. 4. Abbreviations as in Fig. 2

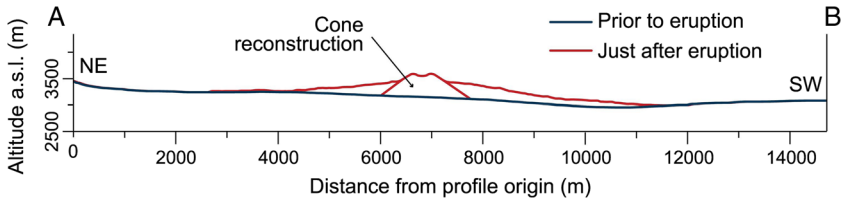

Fig. 4 Elevation profiles of the surface just after the eruption (post-eruptive surface) and the reconstructed topography prior to the eruption (pre-eruptive surface) across Pelado volcano in a northwest-southeast direction. Based on the profiles, a reconstruction of the main cone is shown. For location of the profiles see Fig. 3

covered by lava was estimated through the reconstruction of the post-eruptive surface at 102 km^2.

Tephra deposits

The composite type section of Pelado tephra deposits consists of three main tephra units: basal, middle, and upper. These are composed of 14 distinct strata that we briefly describe here following the terminology of Houghton and Wilson (1989) and White and Houghton (2006). A more detailed description is reported in Lorenzo-Merino (2016). Contacts between strata are in general conformable and stratification is horizontal, consistent with tephra fallout, and any local disruption of the stratification can be attributed to reworking by wind or water, the latter mostly affecting deposits emplaced on sloping ground. The tephra is exclusively made of juvenile clasts, and no xenoliths were found. These clasts cover a continuous range in morphology, crystallinity, and vesicularity that was subdivided into three categories: sideromelane, tachylite, and dense clasts (Table 1; Figs. 5 and 6).

The base of the section is underlain by a paleosol below which two characteristic pumice fallout layers are commonly found: the "Grey Pumice" and the "Tutti-Frutti Pumice" (Fig. 7). These were deposited during the ca. 17,000 calibrated (cal) years before present (BP) Plinian eruption of Popocatépetl and form marker beds across the SCVF (Siebe et al. 2004a, 2005; Sosa-Ceballos et al. 2012; Guilbaud et al. 2015). The Tutti-Frutti Pumice is typically 15-cm thick and readily identified by its milky to orange colors, mild to high degrees of alteration, cm-size pumice clasts, and multicolored lithic fragments dominantly of granodiorite and metamorphic rocks. The underlying Grey Pumice is finer-grained, usually altered to clay, and has an irregular thickness of 2–7 cm across the study area.

Pelado's Basal Tephra Unit (BTU) comprises three strata (B, C, D) that vary from massive to internally stratified, and are composed of loose, well-sorted tephra that ranges from coarse ash to medium lapilli in size (mode coarser than 1φ) (Figs. 7 and 8). The clasts are moderately to highly vesicular (40–65 vol.%) for the most part and dominated by the sideromelane type (Fig. 7). In the type location for this unit (site 21, Fig. 2), grading is normal in stratum B, reverse in C, and absent in D, but this varies across the study area. In addition, stratum B contains thin platy clasts (1–2.5-cm long, 2–5-mm thick) with a grooved and ridged surface.

Transition to the Middle Tephra Unit (MTU) is sharp and marked by a significant reduction in mean grain size (mode finer than 1φ) (Figs. 7 and 8). As shown in Fig. 8, MTU comprises two thinly stratified strata of slightly different color. One is pinkish to dark gray (E), and the other is brown (F). Both have no apparent grading and are composed of well-sorted, mildly to highly indurated tephra that ranges from fine to coarse ash in size. Clasts are in general incipiently to poorly vesicular (15–40 vol.%). Tachylite type clasts are predominant, with lower amounts of the dense type and scarce sideromelane type (Fig. 7). This unit is subdivided by a laterally discontinuous stratum (EF) that unconformably cuts stratum E in the northeast (mostly). This layer is poorly sorted, cross stratified, and contains loose vesicular clasts, similar to those from BTU that are up to fine lapilli in size (Fig. 7).

Table 1 Characteristics of the three main clast types found in Pelado tephra. The typical vesicularity of the different clast types was calculated digitally by drawing vesicle outlines on backscattered electron images of representative clasts, and then measuring their cumulative area% coverage using Adobe Photoshop ®. Crystallinity as seen in backscattered electron images. *ml* microlite, *mp* microphenocrysts

Clast type	Color, transparency	Shape	Vesicularity	Vesicle shape	Crystallinity
Sideromelane	Honey, translucent	Irregular, fluidal to spongy	40–65 vol.%	Large, irregular, some coalesced, up to 200 μm in size	Glassy matrix, scarce ml and mp
Tachylite	Dark brown, opaque	Ridged and jagged, blocky	15–40 vol.%	Small, isolated, subrounded, up to 100 μm in size	Hypo- to holo-crystalline matrix, abundant mp and ml
Dense	Black, opaque	Angular, blocky	0–15 vol.%	Very small, isolated, rounded, up to 25 μm in size	Mainly holocrystalline, abundant mp and ml

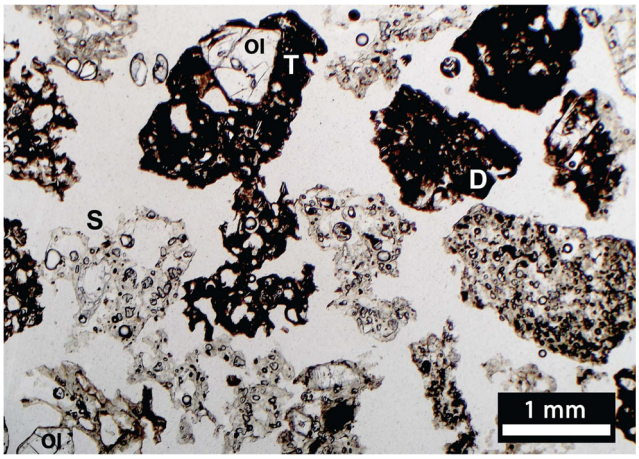

Fig. 5 Tephra clasts under polarizing microscope. S glassy sideromelane with large coalesced vesicles, T tachylite with devitrified glass matrix and smaller isolated vesicles, D dense clast with devitrified glass matrix and scarce very small vesicles, Ol olivine phenocrysts

A distinct, thin (< 2 cm), and reddish layer (stratum G) marks the base of the Upper Tephra Unit (UTU) (Figs. 7 and 8) and is so ubiquitous and unique as to allow its use as a marker layer (Online Resource 1). UTU is composed of a thick, homogeneous sequence of thinly stratified, well- to very well-sorted tephra that alternates between packages of slightly coarser, darker, moderately indurated layers (strata H, K, M, and O) and packages of slightly finer, lighter in tone, highly indurated layers (strata J, L, and N) (Fig. 8). Tephra varies from fine to medium ash in size and is on the whole incipiently vesicular (0–20 vol.%). The componentry of the finer strata is similar to MTU, but clasts in coarser strata are generally denser (Fig. 7).

Lava-tephra stratigraphic relations

Lava-tephra stratigraphic relations could be observed at a deep quarry at the eastern limit of the lava shield (Parres quarry: sites 82 and 83, Fig. 2), road cuts across the south-southeast distal flows (site 57) and northeast of the cone (site 93) along with LIDAR images of the vent area.

Parres quarry

The Parres quarry cuts through Pelado's lavas and tephra deposits and exposes underlying formations. These underlying units consist, from base to top, of a thick lava sequence covered by 2.4-m thick coarse tephra (probably from Acopiaxco volcano located directly upslope: AC in Fig. 2), followed by Popocatepetl's Tutti-Frutti and Grey Pumice layers, with a paleosol in between. There is also a paleosol between all these units and the deposits from Pelado (Fig. 9).

The lowermost part of the Pelado sequence consists of well-stratified, loose, and highly vesicular tephra corresponding to the entire BTU and the base of MTU. This deposit is overlain unconformably by a 3-m thick, massive, olivine-bearing, moderately to highly vesicular (10–20 vol.%), and fractured lava flow unit that is denominated hereafter as the Lower Flow Unit (LFU). LFU can only be found outcropping along the west-southwest and south-southeast limits of the lava flow field (i.e., at sites 84 to 87 and sites 57 and 94 in Fig. 2, respectively). This unit corresponds to the base of the shield.

Directly over LFU (with no paleosol in between) lies a sequence of tephra layers that correlate with strata G to M of UTU. More tephra is deposited over strata M but it is slightly deformed (probably due to the weight of the overlying lava) and hence its correlation with the composite stratigraphic column could not be firmly established. This tephra sequence is overlain by a ~ 12-m thick lava flow unit that is not covered by any appreciable layer of tephra. This lava is clearly different from LFU and was named Upper Flow Unit (UFU). UFU contains orthopyroxene but not olivine, it is moderately to poorly vesicular (0–10 vol.%), has a discontinuous blocky carapace, and shows "onion-type" internal foliation, as defined by James (1920). This unit can be found throughout the central part of the lava field and corresponds to the top of the shield. Its description fits that of the lava samples analyzed by Siebe et al. (2004a, b).

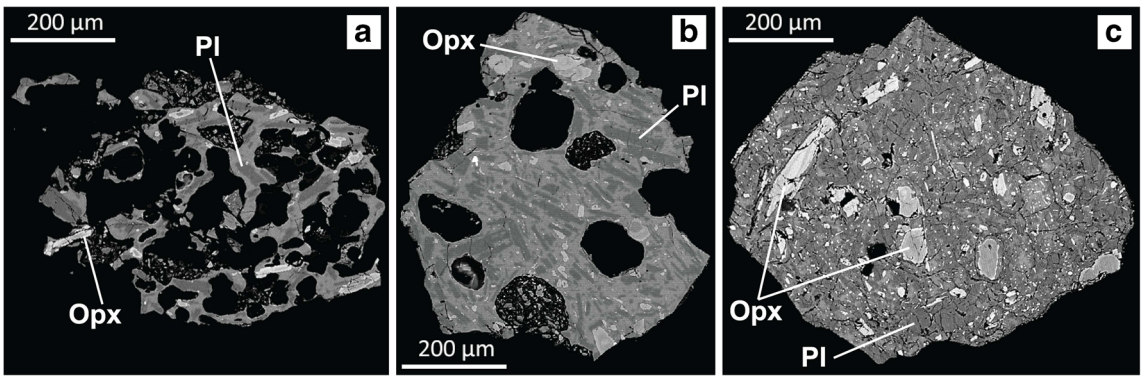

Fig. 6 Backscattered electron microscope images of tephra fragments. **a** Highly vesicular sideromelane. **b** Poorly vesicular tachylite. **c** Incipiently vesicular dense clast. Note the concomitant decrease of vesicularity and increase in microlite content from sideromelane to dense clast. Opx orthopyroxene, Pl plagioclase

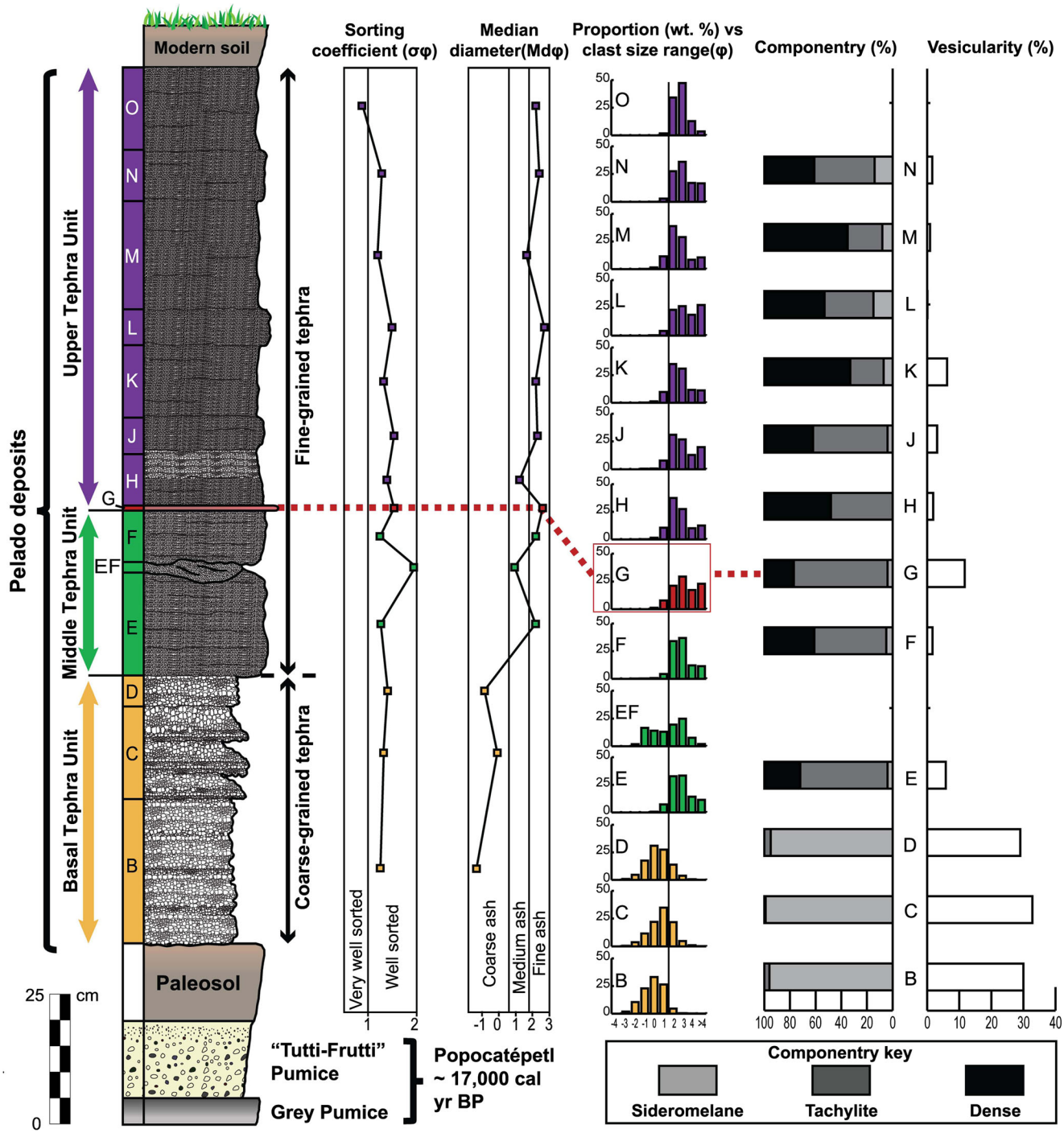

Fig. 7 Type section of Pelado tephra deposits. From left to right: stratigraphic column showing a strata competence profile (with the wider strata as the more competent and vice versa) and variations of sorting, coarseness (median diameter), grain-size distribution, componentry, and average vesicularity of the dominant size fraction (mode). Componentry and vesicularity analyses were not carried out in stratum EF due to its nature as a reworked layer and stratum O due to the high alteration of the clasts. Calibrated radiocarbon age for Popocatépetl products from Sosa-Ceballos et al. (2012)

South-southeast and northeast road cuts

At site 57 located 5 km south-southeast from the vent (Fig. 2), tilted surface lava blocks are covered by 35 cm of stratified tephra (Online Resource 1). The tephra is indurated at the contact with the lava and there is no paleosol between the lava and the tephra. The tephra consists of the upper part of MTU (the uppermost part of stratum E and the entirety of stratum F) overlain by UTU, which is marked by red stratum G at its base. The tephra sequence lies directly on top of moderately

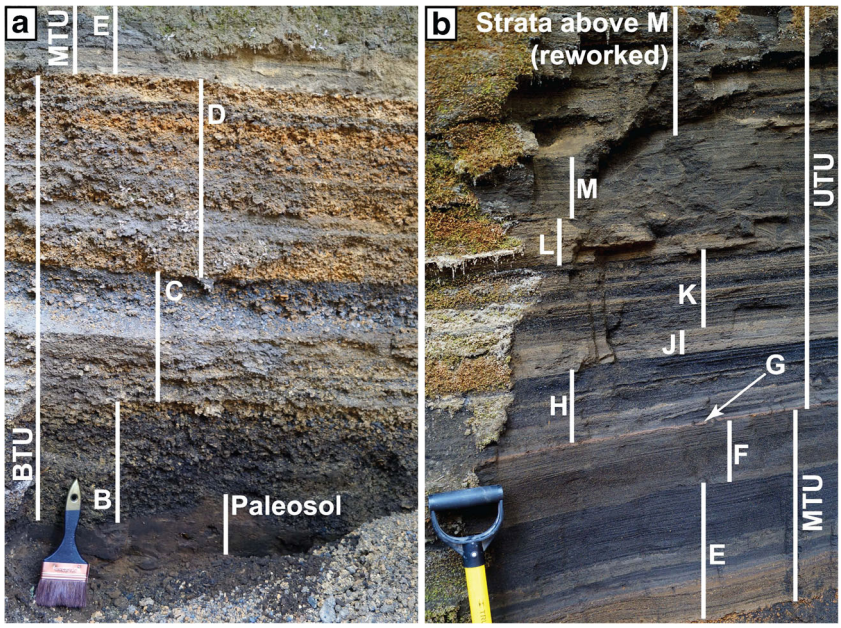

Fig. 8 Representative section across Pelado's tephra sequence (site 80, Fig. 2; Online Resource 1). **a** Detail of BTU and the lower part of MTU with a paleosol underlying the tephra. **b** Detail of MTU and UTU. Note the reddish color of stratum G. The uppermost part of the section shows signs of reworking, and strata N and O cannot be clearly identified at this site

to highly vesicular (10–20 vol.%) olivine-rich lava belonging to LFU. At site 93 (Fig. 2), 700 m northeast of the base of the main summital cone (Pelado proper), poorly vesicular (0–5 vol.%) lava belonging to UFU is covered by 141 cm of tephra from UTU (stratum L to N).

Vent area

LIDAR images of the vent area (Fig. 10) reveal that the last lavas emitted during the eruption were issued from two "bocas" or lateral vents located on the east and west sides of the main summital cone (Pelado proper). The lavas emitted to the west buried a significant part of the smaller summital cone (Tzotzocol), which by this time in the eruption had become inactive. The surface of these lavas has a fresher aspect, with sharper ridges and grooves than the rest of the lavas surrounding the vent area. This suggests that they are not covered by significant amounts of ash. It is hence the last product of the eruption.

Distribution of tephra deposits and isopach maps

The isopach maps made for each unit of the tephra stratigraphic column (BTU, MTU, and UTU) are shown on Fig. 11. They indicate a main dispersal axis to the northeast of the main cone, with a secondary, weaker direction to the southeast. It is worth noting that although thick, almost entirely reworked, massive to cross-stratified tephra deposits were found throughout the mapped area (Fig. 2), exposures of mostly undisturbed primary deposits were found almost exclusively in the deep road cuts to the south and east of the lava shield (Fig. 2). Such deposits were not found to the west of the shield but, in the northwest area, younger Xitle deposits lying over unidentified older deposits can be seen, indicating that, if any of Pelado's ash was deposited in this area, it was too thin to be preserved (< 10 cm).

Two sections with substantially thicker strata in comparison to neighboring sites were found on the steep southeast-facing outer slopes of older, pre-existing scoria cones surrounding the Pelado shield: site 55 over the La Cima scoria cone and site 01 over the Caldera El Guarda scoria cone (Fig. 2; Online Resource 1). Here, deposits locally show cross stratification, fill canals in underlying beds, and thin out laterally. These features indicate substantial syn-eruptive reworking.

Tephra and lava eruptive volumes

Shield volume estimate

Through multiplying the area of lava coverage by the average thickness of flows at the shield margins, Martin del Pozzo (1982), Arana-Salinas (1998), and Siebe et al. (2004a) estimate Pelado's bulk shield volume to be 1–2 km^3. However, this approximation is probably an underestimation due to the considerable accumulation of lava near the vent at this, relatively steep-sided, andesitic shield. As an example, we know that the base of the Paricutin cone is buried under ~ 200 m of lava, whereas the flows at the margin are, in most cases, less than 10-m thick (Luhr and Simkin 1993). At Pelado, the absence of near-vent surface exposures of older cones and/or lavas indicates that proximal lavas must be > 100-m thick. On the other hand, the 10 km^3 bulk volume estimate of Márquez et al. (1999) for Pelado is likely too high because it

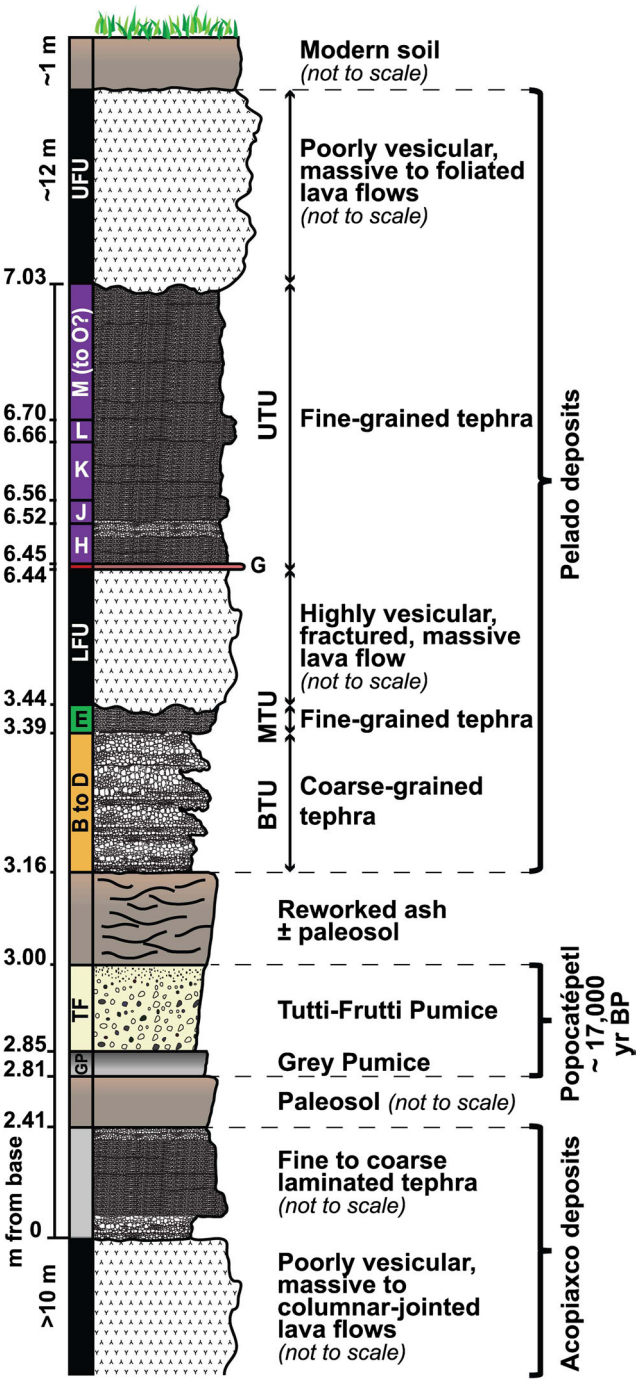

Fig. 9 Complete stratigraphic section of Parres Quarry. Calibrated age for Popocatépetl products from Sosa-Ceballos et al. (2012)

assumes a cone-shaped shield with a flat base, not considering the general topographic gradient.

Based on a careful reconstruction of pre- and post-eruptive surfaces, we calculated an intermediate bulk volume of 6.1 km^3 for the shield (note that this estimate includes summital cones). The distal part of the lavas that was covered by younger volcanoes (21.6 km^2) only accounts for 0.1 km^3 of this total volume, consistent with their low thickness.

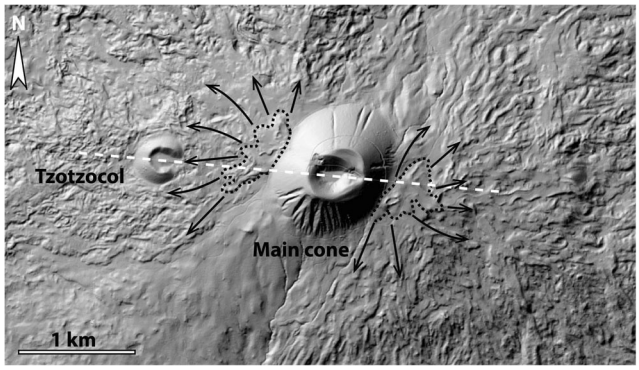

Fig. 10 LIDAR-based digital elevation model of the Pelado vent area. Black dotted lines enclose the areas of lateral lava emission from bocas at the base of the main cone, which are marked by collapse features and possibly caused by lava draining out, marked with arrows. A white dashed line marks the alignment of the vents

Tephra volume estimate

The total volume of the summital cones was calculated at 0.5 km^3 for Pelado proper and 0.05 km^3 for Tzotzocol. For comparison, the volume of the exposed part of the summital cones was estimated at 0.08 km^3 for Pelado proper and 0.01 km^3 for Tzotzocol, hence representing < 20 vol.% of the total edifices. The minimum volume of the distinct tephra units was estimated at 0.3 km^3 for BTU, 0.4 km^3 for MTU, and 0.4 km^3 for UTU (total of ~ 1 km^3).

Dense-rock equivalents (DRE)

The volume of tephra in DRE was calculated to be 0.3 km^3 for the Pelado summital cone, 0.03 km^3 for the Tzotzocol summital cone, and 0.6 km^3 for the medial to distal units (total of ~ 0.9 km^3), considering a bulk deposit density of 1460 kg/m^3 (average for Paricutin from Pioli et al. 2008) and a dense magma density of 2400 kg/m^3 for andesite (Pyle 2000). The volume of lava in DRE was estimated at 5.6 km^3, assuming an average vesicularity of 7 vol.% (Siebe et al. 2004b), a dense magma density of 2400 kg/m^3 for andesite (Pyle 2000), and subtracting the total summital cone bulk volume (0.5 km^3) from the bulk "shield-and-summit-cones" volume (6.1 km^3).

The total erupted volume hence amounts to ~ 6.5 km^3 DRE, 85 vol.% being lava and 15 vol.% tephra. For comparison, tephra formed 61 vol.% of the total magma erupted at Paricutin (Fries 1953).

Interpretation and discussion

We here reconstruct the eruptive activity of Pelado volcano, combining our results with observations made during recent eruptions at monogenetic volcanic fields, in particular the well-documented 1943-52 eruption of Paricutin volcano in

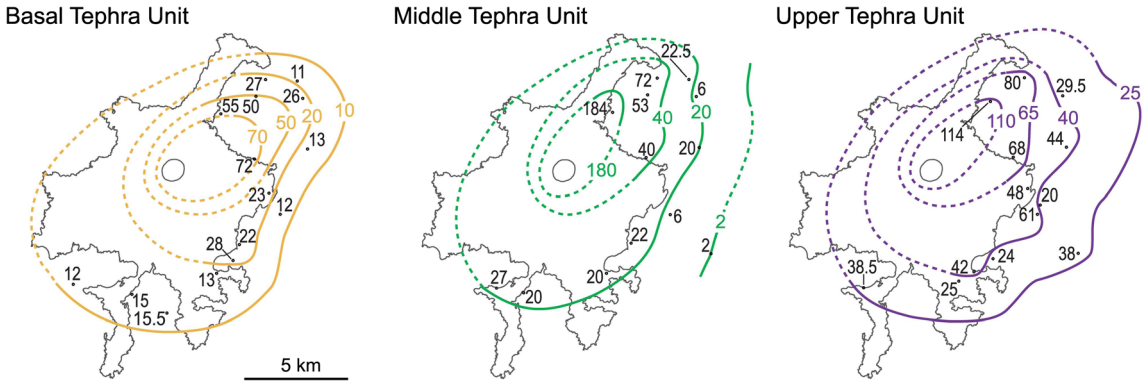

Fig. 11 Isopach maps for the three main tephra units of Pelado volcano. Isopach thicknesses are in cm. Details of the stratigraphic sections that form the basis for these maps can be found in Online Resource 1

central-western México as collated in Luhr and Simkin (1993).

Evidence for monogenetic behavior and syn-eruptive reworking

Our detailed study of the lava and tephra from Pelado volcano shows that this volcano was built during a single eruption, defined here as a series of closely spaced eruptive events without long pauses (> 1 year) between them during which soils and major erosional discordances could have formed. No major discontinuities and soil horizons occur in Pelado's tephra sequence. Locally, unconsolidated deposits show partial to complete reworking at different levels of the sequence, but the only correlatable discontinuity in indurated tephra sections within the eruption sequence is a thin, lenticular, and cross-stratified layer (stratum EF) in MTU unit that contains coarse clasts similar to those of BTU. These structures are indicative of reworking processes taking place at distinct stages of the eruption, but their local nature implies a brief event rather than many events that could affect a surface in many places over a long period of quiescence. Syn-eruptive reworking does not indicate a significant time break as unconsolidated tephra is easily eroded. For example, erosion and tephra removal at Paricutin were intense during the rainy summer season of the first 2 years of activity, resulting in a wide range of laharic products (Segerstrom 1950). Although climatic conditions at the time of Pelado's eruption are poorly known, the presence of large lahar deposits of similar age in the Mexico basin, combined with paleoclimatic data suggest humid conditions at the time (Siebe et al. 1999).

Surface winds could have caused reworking at more local scales. They can generate high-turbulence processes in the lower troposphere, i.e., between the surface and 5 km in altitude, which contribute to long-distance particle transport and the deposition of such particles downwind of topographic barrier (Stull 1988; Baines 1995; Watt et al. 2015). Such processes could in part explain the anomalously thickened sections at sites 01 and 55 (Online Resource 1), because these occur on the downwind side of older cones (Fig. 2). Reworking of unconsolidated tephra deposited on steep slopes is also a likely process at these two locations.

In humid conditions, plants can develop quickly (even less than a year) on loose material such as unconsolidated tephra, which can be completely re-vegetated in only 10 years (e.g., Smathers and Mueller-Dombois 1974; Thornton 2000; Dale et al. 2005). Because there is no evidence of biological reworking in between the units, we must conclude that there were no significant time gaps (> 1 year) during the eruption.

Timing of eruptive events

Early eruptive stage

The approximate east-west alignment of the two summital scoria cones and the location of the lateral vents at the base of the main summital cone (Fig. 10) indicate that magma feeding the eruption ascended along a fissure that was at least the length of the distance between the two summital cones (1.5 km). The smaller Tzotzocol summital cone was not initially attributed to the Pelado eruption, despite its nearly identical chemical composition to the lava shield (Table 2C in Siebe et al. 2004b). Its composition and occurrence along this alignment, which coincide with the main orientation of volcanic and tectonic structures in the SCVF (Marquez et al. 1999), strongly supports the hypothesis that Tzotzocol grew during Pelado's eruption. Unfortunately, though, there are no outcrops exposing the interior of this cone, so its specific place in the overall stratigraphy cannot be established with certainty.

The base of the Pelado sequence is made up of coarse vesicular tephra (BTU, Fig. 7). Thus, in the early stage, activity appears to have been purely explosive, probably associated with the opening of the fissure. However, simultaneous or alternating effusive activity cannot be completely discarded due to lack of exposure of the base of the sequence (strata B to D) close to the vent. For example, lava started flowing as

early as the second day of the eruption at Paricutin, but this lava was entirely buried by later flows (Luhr and Simkin 1993).

The high vesicularity of the tephra, absence of xenoliths, and pervasive parallel stratification indicate that the eruption was triggered by dry magmatic processes and that the initial phase was characterized by fallout. However a phreatomagmatic phase cannot be excluded, because there are no near-vent tephra exposures where deposits of pyroclastic density currents produced by magma-water interaction may be present. Some distal tephra deposits at Pelado were interpreted by Arana-Salinas (1998) as products of pyroclastic density currents, but this was later discarded by detailed field observations from Siebe et al. (2004a), who re-interpreted them as fallout deposits.

The coarseness of the tephra points to weak to medium explosions, where large bombs and agglutinates would have been deposited less than 100 m from the vent. These proximal deposits probably formed elongated pyroclastic ridges that developed, with time, into the summital scoria cones. At this stage, several emission points may have been active at the same time along the fissure. This, combined with variations in explosive intensity and frequency, as well as wind direction, can explain the diffuse and variable stratification of the deposits (Valentine and Gregg 2008).

Intermediate stage

Stratigraphic evidence at Parres quarry indicates that lava emission followed the initial explosive phase, depositing olivine-bearing lavas (LFU), while simultaneous explosive activity formed MTU (most of MTU is absent at the quarry but is complete at site 80, a nearby exposure outside of the lava field, Fig. 2; Online Resource 1). Compared with BTU, the layers that make up MTU are more regular, distinctly thinner, and composed of finer material, suggesting a rhythmic succession of more energetic explosions (greater degree of fragmentation) separated in time (well-defined internal stratification). Another explanation for the change in grain size between BTU and MTU could be a sharp reduction in column height, depositing finer material at the same distance from the vent.

The observed change of main clast type from vesicular sideromelane in BTU to dense tachylite in MTU indicates a change in the physical properties of the magma. Some possible explanations of this change that should be considered for future work include the eruption of a compositionally distinct magma batch, and/or a sharp reduction in magma ascent rates accompanied by partial closure of the fissure that would allow extended times for crystallization and degassing to proceed within the conduit (e.g., Heiken 1978; Taddeucci et al. 2004; D'Oriano et al. 2011). The activity in this stage was probably focused at the two visible summital cones, as eruptions fed by fissures tend to rapidly concentrate into a few points (e.g., Mcdonald 1972; Bruce and Huppert, 1989; Sumner 1998).

While lava flows emitted simultaneously may have come from the center of the summital cones, causing their partial collapse and rafting (e.g., Mcdonald 1972; Gutmann 1979; Valentine et al. 2006), subsequent explosive activity would likely have repaired the breach of these cones, as was witnessed at Paricutin (Foshag and González-Reyna 1956). Alternatively, they may have been emitted from secondary bocas opening at the base of the summital cones, such as those preserved around the main summital cone (Fig. 10). Most of the lavas were emitted in this way at Paricutin where cone-breaching events concentrated in the early eruptive phase when the main cone was small and its walls weak (Luhr and Simkin 1993).

Late eruptive stage

At this stage, the highly regular succession of tephra layers in UTU reflects a stable shallow magmatic system, which can be related to explosive activity essentially focused at the crater of the main summital cone and effusion of UFU lavas from bocas, without significant change in the cone shape. Some lava was directly overlain by the upper part of UTU (as, for example, at site 93, Online Resource 1), indicating coincident explosive and effusive activity at some point in this stage. The absence of bombs and ash on the surface of the last emitted lava flows indicates that the final activity was purely effusive.

Eruptive style

As argued below, our study of Pelado volcano suggests that it erupted in a "violent Strombolian" style, since it shares various features with this type of eruptions, in particular that of Paricutin (1943–1952). The term "violent Strombolian" was introduced by MacDonald (1972) just to describe activity at Paricutin, and has since been applied to a number of other cone-forming eruptions such as Jorullo (Rowland et al. 2009), Pelagatos (Guilbaud et al. 2009) and Xitle (Taddeucci et al. 2011) in Mexico, Cerro Negro in Nicaragua (Hill et al. 1998), and Croscat in Spain (Cimarelli et al. 2010). It has also been used to describe some eruptions at stratovolcanoes, such as those of Llaima in Chile (Ruth and Calder 2013) and Etna and Vesuvius in Italy (Andronico et al. 2009; Arrighi et al. 2001). These eruptions are characterized by a widespread distribution of tephra, high fragmentation index, occurrence of plate tephra, high eruptive column, and simultaneity of explosive and effusive activity.

As at Paricutin and Jorullo, Pelado tephra has a markedly higher fragmentation index when compared with classic Strombolian type eruptions of similar dispersal areas (Fig. 12; Walker 1973; Rowland et al. 2009). In addition, BTU contains "plate tephra," as also found at Paricutin (Foshag and

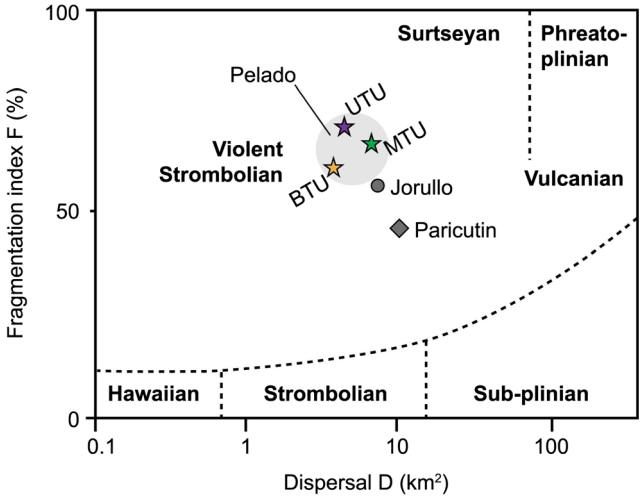

Fig. 12 Pelado tephra data plotted in Dispersal Area versus Fragmentation Index graph after Walker (1973). Data from Paricutin (Walker 1973) and Jorullo (Rowland et al. 2009) are plotted for comparison. Dispersal was calculated as the area in km^2 enclosed by isopach $0.01T_0$ and the fragmentation index as the percentage of tephra under 1 mm in size (0φ) where isopach $0.1T_0$ intercepts the main dispersion axis (Walker 1973). T_0 represents the maximum hypothetical deposit thickness and is obtained from the isopach map

González-Reyna 1956), Pelagatos (Guilbaud et al. 2009), and Llaima (Ruth and Calder 2013). At the latter site, such clasts were interpreted to be fragments of the highly stretched walls of large gas bubbles that ruptured in the vent during the early phase of the 2008–2009 eruption (Ruth and Calder 2013).

At Paricutin, explosions were sufficiently frequent (up to 120/min) to form sustained columns up to 8-km high above the cone (Foshag and González-Reyna 1956). Column heights could not be estimated at Pelado due to the restricted distribution of tephra exposures. Nevertheless, the dispersal axes (Fig. 11) coincide with current high-wind (altitudes > 5.5 km m.a.s.l.) patterns in the area (de Foy et al. 2005), which we interpret as the minimum height of the ash column at Pelado.

Another characteristic feature at Paricutin was the simultaneity in explosive and effusive activity, focused respectively at the crater and base of the main cone (Krauskopf 1948; Bullard 1947; Luhr and Simkin 1993). Our observations suggest that such phenomena also took place at Pelado, although the activity was distributed over a wider area, due to a longer fissure (the original fissure at Paricutin was only 50-m long; Foshag and González-Reyna 1956). Also, similar to Paricutin (Fries 1953; Pioli et al. 2008), tephra/lava production rates appear to have decreased with time at Pelado, along with an increase in the abundance of dense tephra fragments.

Implications for hazards

Hazards linked to monogenetic activity are poorly constrained along the Trans-Mexican Volcanic Belt. Siebe et al. (2004a) detail the possible effects that re-activation of monogenetic volcanism in the central part of the Sierra Chichinautzin would have on the local infrastructure in the region (e.g., impact on main roads, sewer system, electrical power, airports, water supply, etc.), where there would be severe impacts on three major cities: Mexico City (population 21,892,724), Toluca (population 489,333), and Cuernavaca (population 338,650) (INEGI 2010). Our new results help to further constrain the extent of the impact and nature of hazards associated with an eruption similar to that of Pelado, were it to happen in the future.

Lava flows would cause total destruction of a large area around the vent (~ 100 km^2). If occurring in a nearly flat area (i.e., the central part of SCVF), the eruption would probably form a shield with a radius of up to 5 km. If erupted on steep topographic terrain (i.e., the northern or southern limits of the elevated plateau where the SCVF is located), lava flows could form elongate flow fields (over 10 km in length) and reach basins occupied by cities such as Mexico City and Cuernavaca, which are located north and south of the SCVF, respectively. Damage and impacts would follow the scenarios of Trusdell (1995), Felpeto et al. (2001), and Bonne et al. (2008).

Tephra would cause a series of impacts depending on distance from the vent (Blong 1984; Connor et al. 2001; Houghton et al. 2006). Damages to buildings and infrastructure would be most severe within 5 km of the vent due to deposition of a tephra blanket > 150-cm thick. Impacts could be mitigated by implementing an intensive tephra-cleaning program at distances of 5 to 10 km from the vent (50–150-cm thick tephra). A regular cleaning program would be sufficient at a 10–25-km distance from the vent (10–50-cm thick tephra). Examples of tephra-cleaning operations are described in Magill et al. (2013) and Hayes et al. (2017).

Plants and crops would be covered and destroyed up to 10 km from the vent, as vegetation only has a chance of survival and recovery under a tephra blanket of ≤ 50 cm (Rees 1979; Antos and Zobel 1985; Dale et al. 2005). Livestock would have to be evacuated because of illnesses and eventual death related to fluorosis, starvation, ash breathing, and progressive grinding of the molars due to consuming tephra-covered vegetation (Rees 1979; Cronin et al. 1997; Wilson et al. 2015).

Air traffic would be severely disrupted as the threshold ground accumulation thickness for road and airport closure is 1 and 0.1 cm, respectively (Houghton et al. 2006; Scaini et al. 2014). If we assume the same conditions as at Paricutin, ash attained a thickness of 0.1 cm 400 km from the vent (Segerstrom 1950; Fries 1953), and therefore, disruption would be extensive. For example, several international airports such as Mexico City, Cuernavaca, and Toluca would need to be closed (albeit temporarily) while cleaning processes of all communication networks would be required (e.g., Johnston et al. 2000; Siebe et al. 2004a; Wilson et al. 2014).

Conclusion

Large andesitic shields with a summital scoria cone are so common along the Trans-Mexican Volcanic Belt that they were assigned the name "Mexican shield" by Hasenaka (1994). This paper presents the first detailed study of one of the youngest of these, Pelado volcano, located in the Sierra Chichinautzin Volcanic Field, and proves that they can be formed during a single eruption involving both intense explosive activity and voluminous effusion of lava. Our data allow the reconstruction of the eruption which we divided in three stages: early, intermediate, and late. The early stage of Pelado's eruption was probably purely explosive and associated with the opening of an east-west trending fissure of at least 1.5 km in length. Based on the grain size and vesicularity of the tephra, explosiveness must have been weak to medium. The intermediate and late stages were mainly effusive and were associated to the formation of the shield itself. Evidences of simultaneous rhythmic vigorous explosive events were also found during these stages. During the early and intermediate stages, multiple vents were active at the same time along the fissure but, during the final stage, the activity focused to the main cone. The late stage ended with effusive activity from two bocas at the base of the main summital cone. In total, the volcano emitted over 0.9 km^3 DRE of tephra and up to 5.6 km^3 DRE of lavas covering a surface area of 102 km^2. The eruption shares various features with documented "violent Strombolian" eruptions, including the widespread distribution of tephra, high fragmentation index, occurrence of plate tephra, high eruptive column, and simultaneity of explosive and effusive activity.

Mapping of Pelado's tephra deposits and lavas presented in this work demonstrates clearly that the hazards associated with the birth of a new Mexican shield volcano could seriously affect areas located within 25 km of the vent. This is a very important issue for large cities built on or near potentially active zones, such as Mexico City. Because monogenetic eruptions initiate over a period of days to weeks after the first seismic precursors (Yokoyama and De la Cruz-Reyna 1990; Houghton et al. 2006; Albert et al. 2016), preparation for such an eventuality must be implemented sooner rather than later so as to mitigate damage and reduce loss (e.g., Chester et al. 2001; Magill et al. 2013; Sparks et al. 2013).

Acknowledgments Institutional and logistic support was provided by the Instituto de Geofísica, Universidad Nacional Autónoma de México (UNAM). Analytical costs were supported by the Dirección General de Asuntos del Personal Académico UNAM-DGAPA projects PAPIIT IN105615 and IN113517 assigned to Marie-Noëlle Guilbaud. The present work was carried out with the aid of a Masters Graduate Fellowship from Consejo Nacional de Ciencia y Tecnología (CONACyT) to Ainhoa Lorenzo-Merino (2014–2016). The authors wish to thank Gustavo Vivó Vázquez for his invaluable help both in the field and with the ArcGIS software, Armando Vázquez Camargo and Nestor López Valdez for fieldwork support, Lilia Arana for analytical assistance at the Laboratorio de Sedimentología Volcánica of the Instituto de Geofísica UNAM, and Carlos Linares for technical assistance in the acquisition of backscattered electron images at the Laboratorio Universitario de Petrología LUP-UNAM. Two anonymous reviewers, Costanza Bonadonna (associate editor), James White, and Andrew Harris (executive editors) provided insightful comments that greatly improved the manuscript.

References

Aguirre-Díaz GJ, Jaimes-Viera MC, Nieto-Obregón J (2006) The Valle de Bravo Volcanic Field: geology and geomorphometric parameters of a Quaternary monogenetic field at the front of the Mexican Volcanic Belt. Geol Soc Am Spec Pap 402:139–154

Agustín-Flores J, Siebe C, Guilbaud M-N (2011) Geology and geochemistry of Pelagatos, Cerro del Agua, and Dos Cerros monogenetic volcanoes in the Sierra Chichinautzin volcanic field, south of México City. J Volcanol Geoth Res 201:143–162

Albert H, Costa F, Martí J (2016) Years to weeks of seismic unrest and magmatic intrusions precede monogenetic eruptions. Geology 44: 211–214

Andronico D, Cristaldi A, Del Carlo P, Taddeucci J (2009) Shifting styles of basaltic explosive activity during the 2002–03 eruption of Mt. Etna, Italy. J Volcanol Geoth Res 180:110–122

Antos JA, Zobel DB (1985) Recovery of forest understories buried by tephra from Mount St. Helens. Vegetatio 64:103–111

Arana-Salinas L (1998) Geología del volcán Pelado. Undergraduate dissertation, Universidad Nacional Autónoma de México

Arce JL, Layer PW, Lassiter JC, Benowitz JA, Macías JL, Ramírez-Espinosa J (2013) $^{40}Ar/^{39}Ar$ dating, geochemistry, and isotopic analyses of the quaternary Chichinautzin volcanic field, south of Mexico City: implications for timing, eruption rate, and distribution of volcanism. Bull Volcanol 75:774

Arrighi S, Principe C, Rosi M (2001) Violent strombolian and subplinian eruptions at Vesuvius during post-1631 activity. Bull Volcanol 63: 126–150

Baines PG (1995) Topographic effects in stratified flows. Cambridge University Press, Cambridge

Blong R (1984) Volcanic hazards: a sourcebook on the effects of eruptions. Academic Press, Sydney

Bloomfield K (1975) A late-Quaternary monogenetic volcano field in central Mexico. Geol Rundsch 64:476–497

Bonadonna C, Costa A (2012) Estimating the volume of tephra deposits: a new simple strategy. Geology 40:415–418

Bonadonna C, Houghton BF (2005) Total grain-size distribution and volume of tephra-fall deposits. Bull Volcanol 67:441–456

Bonne K, Kervyn M, Cascone L, Njome S, Van Ranst E, Suh E, Ayonghe S, Jacobs P, Ernst G (2008) A new approach to assess long-term lava flow hazard and risk using GIS and low-cost remote sensing: the case of Mount Cameroon, West Africa. Int J Remote Sens 29:6539–6564

Bruce PM, Huppert HE (1989) Thermal control of basaltic fissure eruptions. Nature 342:665–667

Bullard FM (1947) Studies on Parícutin volcano, Michoacan, Mexico. Geol Soc Am Bull 58:433–450

Cas RAF, Wright JV (1988) Volcanic successions, modern and ancient. Chapman & Hall, London

Chester DK, Degg M, Duncan AM, Guest JE (2001) The increasing exposure of cities to the effects of volcanic eruptions: a global survey. Environ Hazards 2:89–103

Chevrel MO, Siebe C, Guilbaud M-N, Salinas S (2016a) The AD 1250 El Metate shield volcano (Michoacán): Mexico's most voluminous Holocene eruption and its significance for archeology and hazards. The Holocene 26:471–488

Chevrel MO, Guilbaud M-N, Siebe C (2016b) The ~AD 1250 effusive eruption of El Metate shield volcano (Michoacán, Mexico): magma source, crustal storage, eruptive dynamics, and lava rheology. Bull Volcanol 78:32

Cimarelli C, Di Traglia F, Taddeucci J (2010) Basaltic scoria textures from a zoned conduit as precursors to violent Strombolian activity. Geology 38:439–442

Connor CB, Conway FM (2000) Basaltic volcanic fields. In: Sigurdsson H (ed) Encyclopedia of volcanoes. Academic Press, San Diego, pp 331–343

Connor CB, Hill BE, Winfrey B, Franklin NM, La Femina PC (2001) Estimation of volcanic hazards from tephra fallout. Nat Hazards 2: 33–42

Cronin SJ, Hedley MJ, Neall VE (1997) Agronomic impact of tephra fallout from the 1995 and 1996 Ruapehu Volcano eruptions, New Zealand. Environ Geol 34:21–30

D'Oriano C, Bertagnini A, Pompilio M (2011) Ash erupted during normal activity at Stromboli (Aeolian Islands, Italy) raises questions on how the feeding system works. Bull Volcanol 73:471–477

Dale VH, Delgado-Acevedo J, MacMahon J (2005) Effects of modern volcanic eruptions on vegetation. In: Marti J, Ernst GGJ (eds) Volcanoes and the environment. Cambridge University Press, Cambridge, pp 227–249

Delgado-Granados H (1992) Geology of the Chapala Rift, Mexico. PhD dissertation, Tohoku University

de Foy B, Caetano E, Magaña V, Zitácuaro A, Cárdenas B, Retama A, Ramos R, Molina LT, Molina MJ (2005) Mexico City basin wind circulation during the MCMA-2003 field campaign. Atmos Chem Phys 5:2267–2288

de Silva S, Lindsay JM (2015) Primary volcanic landforms. In: Sigurdsson H (ed) Encyclopedia of volcanoes second edition. Academic Press, San Diego, pp 273–298

Felpeto A, Araña V, Ortiz R, Astiz M, García A (2001) Assessment and modelling of lava flow hazard on Lanzarote (Canary Islands). Nat Hazards 23:247–257

Foshag WF, González-Reyna J (1956) Birth and development of Parícutin volcano, Mexico. US Geol Surv Bull 965-D. US Government Printing Office, Washington, D.C.

Francis PW, Oppenheimer C (2004) Volcanoes. Oxford University Press, Oxford

Fries C (1953) Volumes and weights of pyroclastic material, lava and water erupted by Paricutin volcano, Michoacan, Mexico. Trans Am Geophys Union 34:603–616

Greeley R (1982) The Snake River Plain, Idaho: representative of a new category of volcanism. J Geophys Res 87:2705–2712

Guilbaud M-N, Siebe C, Agustín-Flores J (2009) Eruptive style of the young high-Mg basaltic andesite Pelagatos scoria cone, southeast of México City. Bull Volcanol 71:859–880

Guilbaud M-N, Arana-Salinas L, Siebe C, Barba-Pingarrón LA, Ortiz A (2015) Volcanic stratigraphy of a high-altitude Mammuthus columbi (Tlacotenco, Sierra Chichinautzin), Central México. Bull Volcanol 77:17

Gutmann JT (1979) Structure and eruptive cycle of cinder cones in the Pinacate volcanic field and the controls of Strombolian activity. J Geol 87:448–454

Hasenaka T (1994) Size, distribution, and magma output rate for shield volcanoes of the Michoacán-Guanajuato volcanic field, Central Mexico. J Volcanol Geoth Res 63:13–31

Hasenaka T, Carmichael ISE (1985) The cinder cones of Michoacán-Guanajuato, central Mexico: their age, volume and distribution, and magma discharge rate. J Volcanol Geoth Res 25:105–124

Hasenaka T, Carmichael ISE (1987) The cinder cones of Michoacán-Guanajuato, central Mexico: petrology and chemistry. J Petrol 28: 241–269

Hayes J, Wilson TM, Deligne NI, Cole J (2017) A model to assess tephra clean-up requirements in urban environments. J Appl Volcanol 6:23

Heiken G (1978) Characteristics of tephra from cinder cone, Lassen volcanic national park, California. Bull Volcanol 41:119–130

Hill BE, Connor CE, Jarzemba MS, La Femina PC, Navarro M, Strauch W (1998) 1995 eruptions of Cerro Negro volcano, Nicaragua, and risk assessment for future eruptions. Geol Soc Am Bull 110:1231–1241

Houghton BF, Wilson CJN (1989) A vesicularity index for pyroclastic deposits. Bull Volcanol 51:451–462

Houghton BF, Bonadonna C, Gregg CE, Johnston DM, Cousins WJ, Cole JW, Del Carlo P (2006) Proximal tephra hazards: recent eruption studies applied to volcanic risk in the Auckland volcanic field, New Zealand. J Volcanol Geoth Res 155:138–149

Instituto Nacional de Estadística, Geografía e Informática [INEGI] (2010) Censo de población y vivienda 2010. Instituto Nacional de Estadística, Geografía e Informática, México

James AV (1920) Factors producing columnar structure in lavas and its occurrence near Melbourne, Australia. J Geol 28:458–469

Johnston DM, Houghton BF, Neall VE, Ronan KR, Paton D (2000) Impacts of the 1945 and 1995–1996 Ruapehu eruptions, New Zealand: an example of increasing societal vulnerability. GSA Bull 112:720–726

Krauskopf KB (1948) Lava movement at Parícutin volcano, Mexico. Geol Soc Am Bull 59:1267–1284

Kshirsagar P, Siebe C, Guilbaud M-N, Salinas S, Layer PW (2015) Late Pleistocene Alberca de Guadalupe maar volcano (Zacapu basin, Michoacán): stratigraphy, tectonic setting, and paleohydrogeological environment. J Volcanol Geoth Res 304:214–236

Le Corvec N, Spörli KB, Rowland J, Lindsay J (2013) Spatial distribution and alignments of volcanic centers: clues to the formation of monogenetic volcanic fields. Earth-Sci Rev 124:96–114

Lorenzo-Merino A (2016) Historia eruptiva del volcán Pelado (Sierra Chichinautzin, México). Master's dissertation, Universidad Nacional Autónoma de México

Lugo-Hubp J (1984) Geomorfología del Sur de la Cuenca de México (Serie Varia 1). Instituto de Geografía UNAM, Ciudad de México

Luhr JF, Simkin T (1993) Parícutin: the volcano born in a Mexican cornfield. Geoscience Press, Phoenix

MacDonald GA (1972) Volcanoes. Prentice-Hall, Englewood Cliffs

Magill C, Wilson TM, Okada T (2013) Observations of tephra fall impacts from the 2011 Shinmoedake eruption, Japan. Earth Planets Space 65:677–698

Márquez A, Verma SP, Anguita F, Oyarzun R, Brandle JL (1999) Tectonics and volcanism of Sierra Chichinautzin: extension at the front of the Central Trans-Mexican Volcanic belt. J Volcanol Geoth Res 93:125–150

Martin del Pozzo AL (1982) Monogenetic volcanism in Sierra Chichinautzin, Mexico. Bull Volcanol 45:1–24

McGee LE, Smith IE (2016) Interpreting chemical compositions of small scale basaltic systems: a review. J Volcanol Geoth Res 325:45–60

Németh K (2010) Monogenetic volcanic fields: origin, sedimentary record, and relationship with polygenetic volcanism. Geol Soc Am SP 470:43–66

Nemeth K, White JD, Reay A, Martin U (2003) Compositional variation during monogenetic volcano growth and its implications for magma supply to continental volcanic fields. J Geol Soc Lond 160:523–530

Pioli L, Erlund E, Johnson E, Cashman K, Wallace P, Rosi M, Delgado Granados H (2008) Explosive dynamics of violent Strombolian eruptions: the eruption of Parícutin Volcano 1943–1952 (Mexico). Earth Planet Sci Lett 271:359–368

Pyle DM (1989) The thickness, volume and grainsize of tephra fall deposits. Bull Volcanol 5:1–15

Pyle DM (2000) Sizes of volcanic eruptions. In: Sigurdsson H (ed) Encyclopedia of volcanoes. Academic Press, San Diego, pp 263–269

Rasoazanamparany C, Widom E, Siebe C, Guilbaud M-N, Spicuzza MJ, Valley JW, Valdez G, Salinas S (2016) Temporal and compositional

evolution of Jorullo volcano, Mexico: implications for magmatic processes associated with a monogenetic eruption. Chem Geol 434:62–80

Rees JD (1979) Effects of the eruption of Parícutin volcano on landforms, vegetation, and human occupancy. In: Sheets PD, Grayson DK (eds) Volcanic activity and human ecology. Academic Press, New York, pp 249–292

Righter K, Carmichael ISE (1992) Hawaiites and related lavas in the Atenguillo graben, western Mexican Volcanic Belt. Geol Soc Am Bull 104:1592–1607

Roberge J, Guilbaud M-N, Mercer CM, Reyes-Luna PC (2015) Insight into monogenetic eruption processes at Pelagatos volcano, Sierra Chichinautzin, Mexico: a combined melt inclusion and physical volcanology study. Geol Soc SP 410:179–198

Rodríguez SR, Morales-Barrera W, Layer P, González-Mercado E (2010) A quaternary monogenetic volcanic field in the Xalapa region, eastern Trans-Mexican volcanic belt: geology, distribution and morphology of the volcanic vents. J Volcanol Geoth Res 197:149–166

Rossi MJ (1996) Morphology and mechanism of eruption of postglacial shield volcanoes in Iceland. Bull Volcanol 57:530–540

Rowland SK, Jurado-Chichay Z, Ernst G, Walker GPL (2009) Pyroclastic deposits and lava flows from the 1759–1774 eruption of El Jorullo, México: aspects of "violent Strombolian" activity and comparison with Parícutin. In: Thordarson T, Self S, Larsen G, Rowland SK, Hoskuldsson A (eds) Studies in volcanology: the legacy of George Walker, IAVCEI SP 2. Geological Society of London, London, pp 105–128

Ruth DCS, Calder ES (2013) Plate tephra: preserved bubble walls from large slug bursts during violent Strombolian eruptions. Geology 42: 11–14

Scaini C, Biass S, Galderisi A, Bonadonna C, Folch A, Smith K, Höskuldsson A (2014) A multi-scale risk assessment for tephra fallout and airborne concentration from multiple Icelandic volcanoes—part II: vulnerability and impact. Nat Hazard Earth Sys 14:2289–2312

Schaaf P, Stimac J, Siebe C, Macías JL (2005) Geochemical evidence for mantle origin and crustal processes in volcanic rocks from Popocatépetl and surrounding monogenetic volcanoes, central Mexico. J Petrol 46:1243–1282

Segerstrom K (1950) Erosion studies at Parícutin, state of Michoacán, Mexico. US Geol Surv Bull 965-A. US Government Printing Office, Washington

Shane P, Smith I (2000) Geochemical fingerprinting of basaltic tephra deposits in the Auckland Volcanic Field. New Zeal J Geol Geop 43:569–577

Siebe C, Schaaf P, Urrutia-Fucugauchi J (1999) Mammoth bones embedded in a late Pleistocene lahar from Popocatépetl volcano, near Tocuila, central México. Geol Soc Am Bull 111:1550–1562

Siebe C, Rodríguez-Lara V, Schaaf P, Abrams M (2004a) Radiocarbon ages of Holocene Pelado, Guespalapa, and Chichinautzin scoria cones, south of Mexico City: implications for archaeology and future hazards. Bull Volcanol 66:203–225

Siebe C, Rodríguez-Lara V, Schaaf P, Abrams M (2004b) Geochemistry, Sr-Nd isotope composition, and tectonic setting of Holocene Pelado, Guespalapa and Chichinautzin scoria cones, south of Mexico City. J Volcanol Geoth Res 130:197–226

Siebe C, Arana-Salinas L, Abrams M (2005) Geology and radiocarbon ages of Tláloc, Tlacotenco, Cuauhtzin, Hijo del Cuauhtzin, Teuhtli, and Ocusacayo monogenetic volcanoes in the central part of the Sierra Chichinautzin, México. J Volcanol Geoth Res 141:225–243

Smathers GA, Mueller-Dombois D (1974) Invasion and recovery of vegetation after a volcanic eruption in Hawaii. National Park Service scientific monograph series, no. 5. National Park Service, Washington, D.C.

Smith IEM, Blake S, Wilson CJN, Houghton BF (2008) Deep-seated fractionation during the rise of a small-volume basalt magma batch: Crater Hill, Auckland, New Zealand. Contrib Mineral Petrol 155: 511–527

Sosa-Ceballos G, Gardner JE, Siebe C, Macías JL (2012) A caldera forming eruption ~14100 ^{14}C yr BP at Popocatépetl volcano, México: insights from eruption dynamics and magma mixing. J Volcanol Geoth Res 213-214:27–40

Sparks RSJ, Aspinall WP, Crosweller HS, Hincks TK (2013) Risk and uncertainty assessment of volcanic hazards. In: Rougier J, Sparks RSJ, Hill LJ (eds) Risk and uncertainty assessment for natural hazards. Cambridge University Press, Cambridge, pp 364–397

Straub SM, LaGatta AB, Martin-Del Pozzo AL, Langmuir CH (2008) Evidence from high-Ni olivines for a hybridized peridotite/pyroxenite source for orogenic andesites from the central Mexican Volcanic Belt. Geochem Geophy Geosy 9:Q03007

Straub SM, Gómez-Tuena A, Zellmer GF, Espinasa-Pereña R, Stuart FM, Cai Y, Langmuir CH, Martin-del Pozzo AL, Mesko GT (2013) The processes of melt differentiation in arc volcanic rocks: insights from OIB-type arc magmas in the central Mexican Volcanic Belt. J Petrol 54:665–701

Strong M, Wolff J (2003) Compositional variations within scoria cones. Geology 31:143–146

Stull RB (1988) An introduction to boundary layer meteorology. Kluwer Academic Publishers, Dordretch

Sumner JM (1998) Formation of clastogenic lava flows during fissure eruption and scoria cone collapse: the 1986 eruption of Izu-Oshima Volcano, eastern Japan. Bull Volcanol 60:195–212

Taddeucci J, Pompilio M, Scarlato P (2004) Conduit processes during the July–August 2001 explosive activity of Mt. Etna (Italy): inferences from glass chemistry and crystal size distribution of ash particles. J Volcanol Geoth Res 137:33–54

Taddeucci J, Scarlato P, Montanaro C, Cimarelli C, Del Bello E, Freda C, Andronico D, Gudmundsson MT, Dingwell DB (2011) Aggregation-dominated ash settling from the Eyjafjallajökull volcanic cloud illuminated by field and laboratory high-speed imaging. Geology 39:891–894

Thornton IWB (2000) The ecology of volcanoes: recovery and reassembly of living communities. In: Sigurdsson H (ed) Encyclopedia of volcanoes. Academic Press, San Diego, pp 1057–1082

Trusdell FA (1995) Lava flow hazards and risk assessment on Mauna Loa volcano, Hawai'i. In: Rhodes JM, Lockwood JP (eds) Mauna Loa revealed: structure, composition, history, and hazards. Geophys Monogr 92. American Geophysical Union, Washington, DC, pp 327–336

Valentine GA, Connor CB (2015) Basaltic volcanic fields. In: Sigurdsson H (ed) The encyclopedia of volcanoes, second edn. Elsevier, Amsterdam, pp 423–439

Valentine GA, Gregg TKP (2008) Continental basaltic volcanoes—processes and problems. J Volcanol Geoth Res 177:857–873

Valentine GA, Perry FV, Krier D, Keating GN, Kelley RE, Cogbill AH (2006) Small-volume basaltic volcanoes: eruptive products and processes, and posteruptive geomorphic evolution in Crater Flat (Pleistocene), southern Nevada. GSA Bull 118:1313–1330

Vesperman D, Schmincke HU (2000) Scoria cones and tuff rings. In: Sigurdsson H (ed) Encyclopedia of volcanoes. Academic Press, San Diego, pp 683–694

Walker GPL (1971) Compound and simple lava flows and flood basalts. Bull Volcanol 35:579–590

Walker GPL (1973) Explosive volcanic eruptions—a new classification scheme. Int J Earth Sci 62:431–446

Watt SFL, Gilbert JS, Folch A, Phillips JC, Cai XM (2015) An example of enhanced tephra distribution driven by topographically induced atmospheric turbulence. Bull Volcanol 77:35

White JDL, Houghton BF (2006) Primary volcaniclastic rocks. Geology 34:677–680

Whitford-Stark JL (1975) Shield volcanoes. In: Fielder G, Wilson L (eds) Volcanoes of the earth, moon, and Mars. St. Martin's Press, New York, pp 66–74

Williams H, McBirney AR (1979) Volcanology. Freeman and Cooper, San Francisco

Wilson G, Wilson TM, Deligne NI, Cole JW (2014) Volcanic hazard impacts to critical infrastructure: a review. J Volcanol Geoth Res 286:148–182

Wilson TM, Jenkins S, Stewart C (2015) Impacts from volcanic ash fall. In: Papale P (ed) Volcanic hazards, risks, and disasters. Elsevier, Amsterdam, pp 47–86

Wood CA (1980) Morphometric evolution of cinder cones. Volcanol Geoth Res 7:387–413

Yokoyama I, De la Cruz-Reyna S (1990) Precursory earthquakes of the 1943 eruption of Paricutin volcano, Michoacan, Mexico. J Volcanol Geoth Res 44:265–281

Zimmer BW, Riggs NR, Carrasco-Núñez G (2010) Evolution of tuff ring-dome complex: the case study of Cerro Pinto, eastern Trans-Mexican Volcanic Belt. Bull Volcanol 72:1223–1240